PROTEINS
STRUCTURE ■ FUNCTION ■ BIOINFORMATICS

STRUCTURE NOTE

The PR/SET domain in PRDM4 is preceded by a zinc knuckle

Klára Briknarová,[1,2]* Daniel Z. Atwater,[1] Jessica M. Glicken,[1] Stacy J. Maynard,[1] and Tara E. Ness[1]

[1] Department of Chemistry and Biochemistry, The University of Montana, Missoula, Montana 59812

[2] Center for Biomolecular Structure and Dynamics, The University of Montana, Missoula, Montana 59812

Key words: zinc-binding domain; zinc knuckle; PR domain; SET domain; Schwann cell factor 1; PRDM6; PRDM9; meisetz; PRDM10; tristanin.

INTRODUCTION

PR proteins play key roles in various aspects of cell differentiation and organismal development, and, when dysregulated, are involved in carcinogenesis.[1–6] The defining feature of PR proteins is a conserved sequence termed the PR (PRDI-BF1 and RIZ1 homology) domain,[7] which is almost always accompanied by an array of C2H2-like zinc fingers. Other sequences that are present in PR proteins show limited conservation and contain virtually no discernible motifs.

The PR domain is a significantly diverged variant of a SET domain,[8] a motif with protein (often histone) lysine N-methyltransferase activity.[9] However, amino acid sequence identity between PR domains and canonical SET domains is typically less than 25%, and a number of residues that are conserved in canonical SET domains and believed to be important for enzymatic activity are not conserved in PR domains.[1] Hence, it is not surprising that from the 17 PR proteins identified in humans, only two (PRDM2/RIZ1[10] and PRDM9/meisetz[4]) have been demonstrated to have intrinsic histone lysine methyltransferase activity that is detectable in assays using radioactive substrate. Efforts to detect intrinsic methyltransferase activity of other PR proteins have been unsuccessful,[11–13] and hence, it remains to be determined how these proteins carry out their regulatory functions. Several PR proteins have been shown to interact with other transcriptional factors,[7,11–15] and hence, instead of modifying chromatin themselves, they may mediate protein-protein interactions and recruit other proteins (including chromatin modifying enzymes) to chromatin.

PRDM4 (Schwann cell factor 1, SC-1) is a member of the PR protein family.[16] It is a transcriptional regulator that has been implied in transduction of nerve growth factor signals via the p75 neurotrophin receptor and in cell growth arrest[15,17] and is expressed in a variety of tissues including the central and peripheral nervous systems.[16,18] Interestingly, we noticed that the PR domain in PRDM4 is preceded by a short motif that is also present in several other PR proteins including human PRDM6 (PRISM),[13,19] PRDM7,[20] PRDM9 (meisetz),[4,21–23] PRDM10 (tristanin),[24,25] PRDM11, and PRDM15[26] [Fig. 1(A,B)]. The conservation of cysteine and histidine residues suggested that this ~20 amino acid motif binds zinc, and hence, we refer to it as the "PR zinc knuckle" to distinguish it from the longer (~30 amino acid) C2H2-like zinc fingers that are located C-terminally of the PR domain. In addition to identifying this motif, we demonstrate in this report that the PR zinc knuckle indeed coordinates zinc and we present its 3-dimensional structure determined by NMR spectroscopy.

*Correspondence to: Klára Briknarová, Department of Chemistry and Biochemistry, The University of Montana, 32 Campus Drive, Missoula, MT 59812.
E-mail: klara.briknarova@umontana.edu
Received 6 March 2011; Revised 6 April 2011; Accepted 8 April 2011
Published online 20 April 2011 in Wiley Online Library (wileyonlinelibrary.com).
DOI: 10.1002/prot.23057

© 2011 WILEY-LISS, INC.

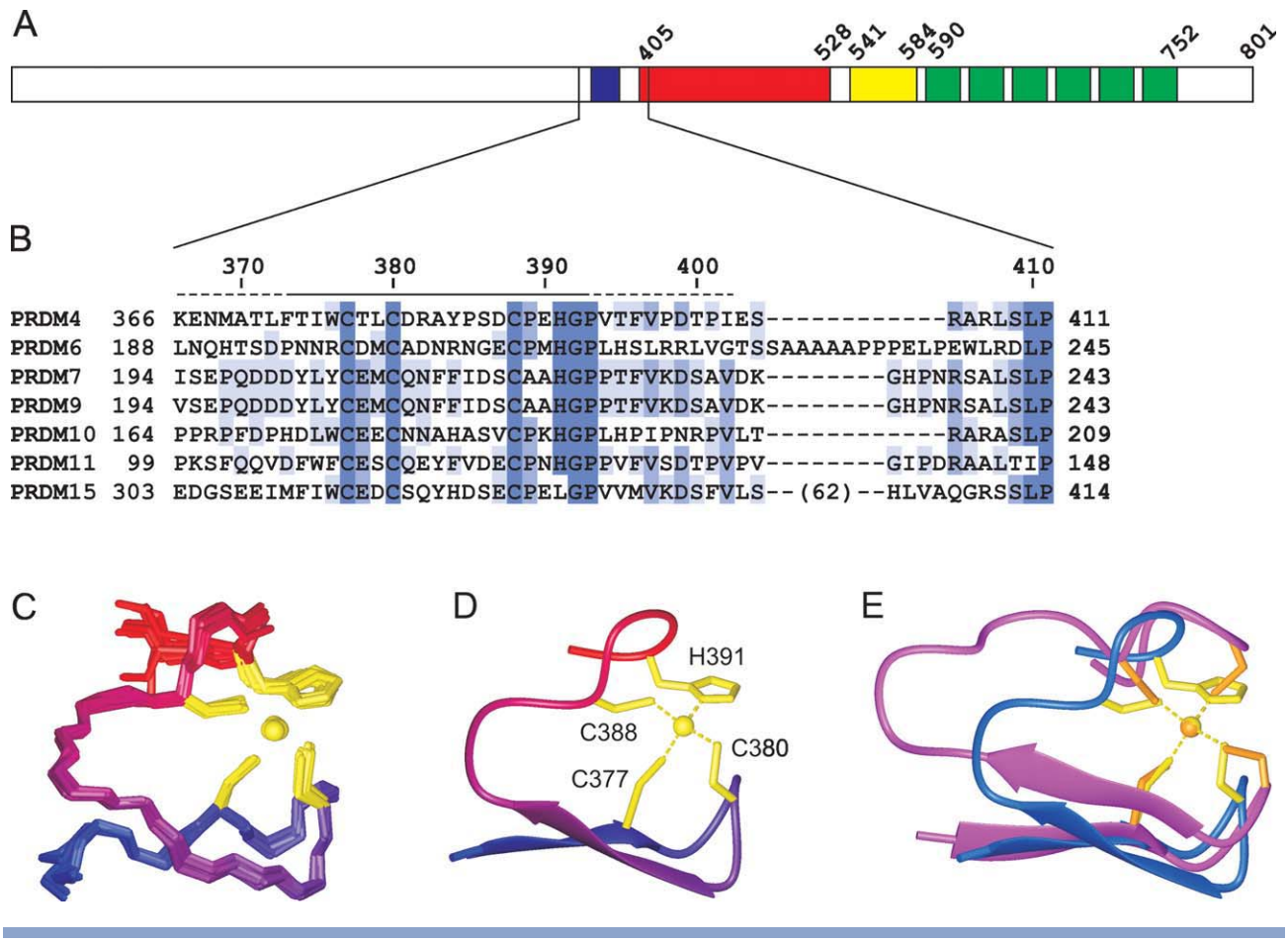

Figure 1

The zinc knuckle in PRDM4. (**A**) A schematic drawing of human PRDM4 with the zinc knuckle motif shown in blue, PR domain in red, cysteine/histidine-rich region in yellow, and C_2H_2-like zinc finger domains in green. (**B**) Alignment of the zinc knuckle and adjacent sequences from human PRDM4 (Q9UKN5), PRDM6 (Q9NQX0), PRDM7 (Q9NQW5), PRDM9 (Q9NQV7), PRDM10 (Q9NQV6), PRDM11 (Q9NQV5), and PRDM15 (P57071). The sequences are colored by percent identity[27] to highlight the C-X_2-C-X_7-C-X_2-H-G-P conserved pattern. PRDM15 sequence lacks the conserved histidine and contains a large insertion between the zinc knuckle and the PR domain, which was omitted for clarity. The span of the recombinant PRDM4(366–402) peptide that was used in this study is indicated above the sequences; the solid line denotes the structured region while the dashed line marks the disordered segments. (**C**) Ten superimposed backbone traces of the zinc knuckle (residues 374–392) from PRDM4. The color changes smoothly from blue at the N-terminus to red at the C-terminus. Cysteine and histidine side chains that coordinate zinc are shown in yellow, and zinc ions are depicted as yellow spheres. (**D**) A ribbon model of the zinc knuckle (residues 374–392) from PRDM4. The coloring scheme is the same as in panel (C). (**E**) A comparison of the zinc knuckle (residues 374–392) from PRDM4 (blue and yellow) with the structurally equivalent portion (residues 724–747) of the RanBP2-type zinc finger from nucleoporin 153 (PDB ID 2K0C; magenta and orange).[28] The structures were superimposed using the zinc ions and the zinc-coordinating atoms.

MATERIALS AND METHODS

Plasmid pCR-PFM1.5, containing the cDNA sequence of human PRDM4, was a gift from Dr. Shi Huang (State Key Laboratory of Medical Genetics, Xiangya Medical School, Central South University, Changsha, Hunan, China). The sequence encoding PRDM4 residues 366–402 was amplified from pCR-PFM1.5 by PCR and cloned into pGEX-4T1 expression vector (GE Healthcare). The PRDM4(366-402) peptide fused to glutathione transferase (GST) was expressed in *Escherichia coli* BL21-CodonPlus(DE3)-RIL cells (Stratagene) and purified by affinity chromatography on glutathione-agarose resin. The GST moiety was subsequently cleaved off with thrombin, and PRDM4(366–402) was separated from thrombin and GST by affinity chromatography on *p*-aminobenzamidine and glutathione-agarose resins, respectively. Finally, the PRDM4(366–402) peptide was concentrated in the buffer used for affinity chromatography (50 m*M* Tris, 100 m*M* NaCl, 5 m*M* β-mercaptoethanol, pH 8.0) supplemented with additional 100 m*M* β-mercaptoethanol, purified by reversed phase high-performance liquid chromatography (HPLC) and lyophilized.

The samples for NMR experiments contained 0.2–0.5 m*M* unlabeled or ^{15}N-labeled PRDM4(366–402), 50 m*M* $^{2}H_{11}$-Tris, 2.5 m*M* $^{2}H_{16}$-TCEP and 1.5–2.5 m*M* $ZnSO_4$ in 90% H_2O/10% $^{2}H_2O$, pH 7.1–7.2, or in $^{2}H_2O$, pH* 7.2 (uncorrected pH meter reading). Air in NMR tubes was replaced with argon to help preserve cysteine residues in the reduced state. 2D double quantum filtered COSY, TOCSY, NOESY, E-COSY, ^{1}H-^{15}N HSQC, ^{1}H-^{15}N HMQC, ^{1}H-^{15}N heteronuclear NOE, 3D ^{15}N-edited TOCSY, ^{15}N-edited NOESY, HNHA, and HNHB experiments were acquired at 25°C on a Varian 600 MHz NMR System equipped with a cold probe. The data were processed and analyzed with Felix 2004 (Accelrys Inc./Felix NMR Inc.), and sequential assignments were obtained using standard procedures.[29]

$^{3}J_{HNH\alpha}$ values were determined from HNHA spectrum, and the ϕ dihedral angles were restrained to the range of $-120° \pm 50°$ for $^{3}J_{HNH\alpha} > 8$ Hz, $-120° \pm 40°$ for $^{3}J_{HNH\alpha} > 9$ Hz, and $-60° \pm 30°$ for $^{3}J_{HNH\alpha} < 5$ Hz. Clear $H^{\alpha(i-1)}$ crosspeaks in HNHB, corresponding to $^{3}J_{NH\alpha(i-1)} < -1.2$ Hz, indicated that N is *trans* to $H^{\alpha(i-1)}$, and the relevant ψ dihedral angles were restrained to $-60° \pm 60°$. Stereospecific assignments of β-methylene protons and χ_1 dihedral angle restraints were based on $^{3}J_{H\alpha H\beta}$ values from E-COSY and $^{3}J_{NH\beta}$ from HNHB spectrum. The individual χ_1 rotamers were restrained to $-60° \pm 30°$, $60° \pm 30°$, and $180° \pm 30°$, respectively. Structure calculations were performed with Aria2.3[30] in conjunction with CNS 1.21[31] and employed a total of 26 dihedral angle (14ϕ, 3ψ, and 9χ_1) restraints and 1050 volumes from 2D NOESY spectrum. Ambiguous distance restraints were generated in Aria from NOESY volumes in an iterative manner and corrected for spin diffusion.[32] Structures were initially calculated without any zinc atoms or constraints for zinc coordination. A cluster of residues posed to coordinate zinc was identified in these preliminary structures, and geometrical constraints to coordinate zinc by this cluster were included in all subsequent calculations. Each Aria calculation yielded 20 structures, 10 of which were refined in explicit water. Six Aria calculations were performed to evaluate convergence and reproducibility, and the statistics for one representative calculation is summarized in Table I. Figures were prepared with the molecular graphics program Molmol 2K.1.[35] The coordinates and chemical shifts have been deposited in the Protein Data Bank (PDB) and Biomagnetic Resonance Bank (BMRB) with ID 2L9Z and 17494, respectively.

Table I
Structural Statistics for PRDM4(366–402)

Experimental restraints	
Volumes from 2D NOESY spectrum	1050
Distance restraints generated from NOESY volumes	
by Aria	648
Intraresidual	211
Sequential	157
Medium range ($2 \leq \|i-j\| \leq 4$)	70
Long range ($5 \leq \|i-j\|$)	122
Ambiguous	88
Dihedral angle restrains	26
ϕ dihedral angle restraints	14
ψ dihedral angle restraints	3
χ_1 dihedral angle restraints	9
Hydrogen bond restrains	0
Root mean square deviation (RMSD) from experimental restraints	
NOE distance restraints (Å)	0.014 ± 0.002
Dihedral angle restraints (°)	0.12 ± 0.09
Number of experimental restraint violations	
NOE violations >0.5 Å	0 ± 0
Dihedral angle violations >5°	0 ± 0
RMSD from idealized geometry[a]	
Bonds (Å)	0.0032 ± 0.0001
Angles (°)	0.49 ± 0.02
Impropers (°)	1.3 ± 0.1
Energy (kcal/mol)	
Total	−1025 ± 31
Bonds	6.1 ± 0.6
Angles	39 ± 4
Improper	18 ± 3
Dihedral	171 ± 2
Van der Waals	−91 ± 8
Electrostatic	−1174 ± 27
NOE distance restraints	6 ± 2
Dihedral angle restraints	0.04 ± 0.04
Distribution of φ, ψ dihedral angles of residues 374–392 in Ramachandran plot[34]	
The most favored regions (%)	76.9
Additional allowed regions (%)	23.1
Generously allowed regions (%)	0.0
Disallowed regions (%)	0.0
RMSD of residues 374–392 from mean coordinates[b]	
Backbone atoms (N, C^{α}, C) (Å)	0.29 ± 0.09
Heavy atoms (Å)	0.67 ± 0.16

[a]Idealized covalent geometry is based on the parallhdg5.3.pro parameters.[33]
[b]Mean coordinates were obtained by averaging coordinates of the 10 calculated structures, which were first superposed using backbone atoms (N, C^{α}, C) of residues 374–392.

RESULTS AND DISCUSSION

Careful sequence comparison revealed that in human PRDM4, PRDM6, PRDM7, PRDM9, PRDM10, PRDM11, and PRDM15, the PR domain is preceded by a short motif with consensus sequence C-X_2-C-X_7-C-X_2-H-G-P where X can be any amino acid [Fig. 1(B)]. A Prosite scan[36] indicated that this consensus sequence is found exclusively in PR proteins and does not match any established Prosite motif.[37] We cloned, expressed, and purified a fragment of human PRDM4 that contains this conserved sequence, and here, we report its structural characterization.

The strict conservation of the cysteine and histidine residues suggested that this motif binds zinc. Indeed, PRDM4(366–402) required addition of a mole equivalent of Zn^{2+} to yield NMR spectra with well-dispersed signals typical of folded proteins (data not shown). The NMR spectra of PRDM4(366–402) in the presence of zinc were amenable to analysis, and we proceeded with resonance assignment and determination of the solution structure

of zinc-bound PRDM4(366–402). In preliminary structures that were calculated without any constraints for zinc coordination, the side chains of the conserved cysteine and histidine residues (C377, C380, C388, and H391) were clustered together and oriented suitably to coordinate a zinc ion. H391 is positioned to coordinate zinc via the Nδ1 atom, consistent with its Nϵ2-H tautomeric state inferred from 2D ^{1}H-^{15}N HMQC spectrum. Residues N-terminal of F373 and C-terminal of P393 are disordered, as indicated by lack of long-range NOEs in 2D NOESY spectrum and by ^{1}H-^{15}N heteronuclear NOE data. Residues 374–392 adopt a compact globular fold that consists of a β-hairpin (two short β-strands, I375-C377 and R382-Y384, connected by a type I β-turn) and a type I β-turn (C388-H391) that cross each other at an angle of ∼40°. The β-hairpin contains two of the zinc-coordinating residues (C377, C380) while the β-turn contains the other two (C388, H391), and the zinc is sandwiched between the β-hairpin and the type I β-turn. The 3D model of residues 374–392 of PRDM4(366–402) with a bound zinc ion is presented in Figure 1(C,D).

The PR zinc knuckle fold is similar to that of Gag-knuckles (a β-hairpin providing two zinc ligands followed by a short helix or a loop providing the other two zinc ligands) and zinc ribbons (two β-hairpins, each providing two zinc ligands).[38] The structure most closely related to the PR zinc knuckle that we identified using SSM search[39] is that of a RanBP2-type zinc finger from nucleoporin 153 (Nup153ZnF2)[28] [Fig. 1(E)], with RMSD between backbone atoms of residues 374–392 of PRDM4 and their counterparts in Nup153ZnF2 1.83 Å. RanBP2-type zinc fingers (PROSITE ID PDOC50199) are defined by the consensus pattern W-X-C-X_{2-4}-C-X_3-N-X_6-C-X_2-C and fold consisting of two short β-hairpins, the second of which may be twisted and lack canonical cross-strand hydrogen bonding.[40–43] Each β-hairpin provides two of the conserved cysteine residues to coordinate zinc. Despite the structural similarity, the PR zinc knuckle is clearly distinct from RanBP2-like zinc fingers. Major differences include zinc coordination by three cysteines and one histidine rather than four cysteines, fewer residues (7 versus 10) between the second and third cysteine, and absence of residues that are well conserved in RanBP2-type zinc fingers (W, N) at the equivalent positions in PR zinc knuckles.

RanBP2-type zinc fingers serve as protein and RNA recognition motifs, mediating interactions with ubiquitin,[44] GTP-binding nuclear protein Ran,[28,43] and single-stranded RNA sequences.[45] It is unlikely that the PR zinc knuckles bind nucleic acids as they display a shortage of positively charged amino acids [Fig. 1(B)] that are typical of RNA/DNA-binding domains. However, it is tempting to speculate that PR zinc knuckles facilitate protein-protein interactions in a manner similar to RanBP2-type zinc fingers. The function of the zinc knuckle in PR proteins awaits further investigation.

ACKNOWLEDGMENTS

The authors are grateful to Dr. Shi Huang for providing them with the pCR-PFM1.5 plasmid and to Dr. Bruce Bowler for making his HPLC system and lyophilizer available to them. The 600 MHz NMR spectrometer at The University of Montana was purchased with funds from NSF grant CHE-0321002 and from the Murdock Charitable Trust. Tara Ness was supported by undergraduate research awards from the Montana Integrative Learning Experience for Students (MILES) program (Howard Hughes Medical Institute Undergraduate Science Education Program grant 52005905 to The University of Montana), National Science Foundation EPSCoR program (grant EPS-0701906 to The University of Montana), and Davidson Honors College. Stacy Maynard was a participant in the Research Experiences for Undergraduates (REU) program at The University of Montana that was funded by NSF grant CHE-0649306.

REFERENCES

1. Huang S. Histone methyltransferases, diet nutrients and tumour suppressors. Nat Rev Cancer 2002;2:469–476.
2. Bikoff EK, Morgan MA, Robertson EJ. An expanding job description for Blimp-1/PRDM1. Curr Opin Genet Dev 2009;19:1–7.
3. Wieser R. The oncogene and developmental regulator EVI1: expression, biochemical properties, and biological functions. Gene 2007; 396:346–357.
4. Hayashi K, Yoshida K, Matsui Y. A histone H3 methyltransferase controls epigenetic events required for meiotic prophase. Nature 2005;438:374–378.
5. Yamaji M, Seki Y, Kurimoto K, Yabuta Y, Yuasa M, Shigeta M, Yamanaka K, Ohinata Y, Saitou M. Critical function of Prdm14 for the establishment of the germ cell lineage in mice. Nat Genet 2008; 40:1016–1022.
6. Seale P, Kajimura S, Yang W, Chin S, Rohas LM, Uldry M, Tavernier G, Langin D, Spiegelman BM. Transcriptional control of brown fat determination by PRDM16. Cell Metab 2007;6:38–54.
7. Buyse IM, Shao G, Huang S. The retinoblastoma protein binds to RIZ, a zinc-finger protein that shares an epitope with the adenovirus E1A protein. Proc Natl Acad Sci USA 1995;92:4467–4471.
8. Jenuwein T, Laible G, Dorn R, Reuter G. SET domain proteins modulate chromatin domains in eu- and heterochromatin. Cell Mol Life Sci 1998;54:80–93.
9. Rea S, Eisenhaber F, O'Carroll D, Strahl BD, Sun ZW, Schmid M, Opravil S, Mechtler K, Ponting CP, Allis CD, Jenuwein T. Regulation of chromatin structure by site-specific histone H3 methyltransferases. Nature 2000;406:593–599.
10. Kim KC, Geng L, Huang S. Inactivation of a histone methyltransferase by mutations in human cancers. Cancer Res 2003;63:7619–7623.
11. Győry I, Wu J, Fejér G, Seto E, Wright KL. PRDI-BF1 recruits the histone H3 methyltransferase G9a in transcriptional silencing. Nat Immunol 2004;5:299–308.
12. Duan Z, Person RE, Lee HH, Huang S, Donadieu J, Badolato R, Grimes HL, Papayannopoulou T, Horwitz MS. Epigenetic regulation of protein-coding and microRNA genes by the Gfi1-interaction tumor suppressor PRDM5. Mol Cell Biol 2007;27:6889–6902.
13. Davis CA, Haberland M, Arnold MA, Sutherland LB, McDonald OG, Richardson JA, Childs G, Harris S, Owens GK, Olson EN. PRISM/PRDM6, a transcriptional repressor that promotes the proliferative gene program in smooth muscle cells. Mol Cell Biol 2006; 26:2626–2636.

14. Yu J, Angelin-Duclos C, Greenwood J, Liao J, Calame K. Transcriptional repression by Blimp-1 (PRDI-BF1) involves recruitment of histone deacetylase. Mol Cell Biol 2000;20:2592–2603.
15. Chittka A, Arevalo JC, Rodriguez-Guzman M, Pérez P, Chao MV, Sendtner M. The p75NTR-interacting protein SC1 inhibits cell cycle progression by transcriptional repression of cyclin E. J Cell Biol 2004;164:985–996.
16. Yang XH, Huang S. PFM1 (PRDM4), a new member of the PR-domain family, maps to a tumor suppressor locus on human chromosome 12q23-q24.1. Genomics 1999;61:319–325.
17. Chittka A, Chao MV. Identification of a zinc finger protein whose subcellular distribution is regulated by serum and nerve growth factor. Proc Natl Acad Sci USA 1999;96:10705–10710.
18. Kendall SE, Ryczko MC, Mehan M, Verdi JM. Characterization of NADE, NRIF and SC-1 gene expression during mouse neurogenesis. Dev Brain Res 2003;144:151–158.
19. Wu Y, Fergusson JE, III, Wang H, Kelley R, Ren R, McDonough H, Meeker J, Charles PC, Wang H, Patterson C. PRDM6 is enriched in vascular precursors during development and inhibits endothelial cell proliferation, survival, and differentiation. J Mol Cell Cardiol 2008;44:47–58.
20. Fumasoni I, Meani N, Rambaldi D, Scafetta G, Alcalay M, Ciccarelli FD. Family expansion and gene rearrangements contributed to the functional specialization of PRDM genes in vertebrates. BMC Evol Biol 2007;7:187.
21. Parvanov ED, Petkov PM, Paigen K. Prdm9 controls activation of mammalian recombination hotspots. Science 2010;327:835.
22. Baudat F, Buard J, Grey C, Fledel-Alon A, Ober C, Przeworski M, Coop G, de Massy B. PRDM9 is a major determinant of meiotic recombination hotspots in humans and mice. Science 2010; 327:836–840.
23. Myers S, Bowden R, Tumian A, Bontrop RE, Freeman C, MacFie TS, McVean G, Donnelly P. Drive against hotspot motifs in primates implicates the PRDM9 gene in meiotic recombination. Science 2010;327:876–879.
24. Siegel DA, Huang MK, Becker SF. Ectopic dendrite initiation: CNS pathogenesis as a model of CNS development. Int J Dev Neurosci 2002;20:373–389.
25. Park JA, Kim KC. Expression patterns of PRDM10 during mouse embryonic development. BMB Rep 2010;43:29–33.
26. Shibuya K, Kudoh J, Okui M, Shimizu N. Identification of a novel zinc finger protein gene (ZNF298) in the GAP2 of human chromosome 21q. Biochem Biophys Res Commun 2005;332:557–568.
27. Waterhouse AM, Procter JB, Martin DM, Clamp M, Barton GJ. Jalview version 2—a multiple sequence alignment editor and analysis workbench. Bioinformatics 2009;25:1189–1191.
28. Schrader N, Koerner C, Koessmeier K, Bangert JA, Wittinghofer A, Stoll R, Vetter IR. The crystal structure of the Ran-Nup153ZnF2 complex: a general Ran docking site at the nuclear pore complex. Structure 2008;16:1116–1125.
29. Wüthrich K. NMR of proteins and nucleic acids. Wiley, New York; 1986. 292 p.
30. Rieping W, Habeck M, Bardiaux B, Bernard A, Malliavin TE, Nilges M. ARIA2: automated NOE assignment and data integration in NMR structure calculation. Bioinformatics 2007;23:381–382.
31. Brünger AT, Adams PD, Clore GM, DeLano WL, Gros P, Grosse-Kunstleve RW, Jiang JS, Kuszewski J, Nilges M, Pannu NS, Read RJ, Rice LM, Simonson T, Warren GL. Crystallography and NMR system (CNS): a new software suite for macromolecular structure determination. Acta Crystallogr 1998;D54:905–921.
32. Linge JP, Habeck M, Rieping W, Nilges M. Correction of spin diffusion during iterative automated NOE assignment. J Magn Reson 2004;167:334–342.
33. Linge JP, Habeck M, Rieping W, Nilges M. ARIA: automated NOE assignment and NMR structure calculation. Bioinformatics 2003;19:315–316.
34. Laskowski RA, Rullmann JA, MacArthur MW, Kaptein R, Thornton JM. AQUA and PROCHECK-NMR: programs for checking the quality or protein structures solved by NMR. J Biomol NMR 1996;8:477–486.
35. Koradi R, Billeter M, Wüthrich K. MOLMOL: a program for display and analysis of macromolecular structures. J Mol Graph 1996;14:51–55.
36. Sigrist CJA, Cerutti L, Hulo N, Gattiker A, Falquet L, Pagni M, Bairoch A, Bucher P. PROSITE: a documented database using patterns and profiles as motif descriptors. Brief Bioinform 2002;3:265–274.
37. Sigrist CJA, Cerutti L, de Castro E, Langendijk-Genevaux PS, Bulliard V, Bairoch A, Hulo N. PROSITE, a protein domain database for functional characterization and annotation. Nucleic Acids Res 2010;38:161–166.
38. Krishna SS, Majumdar I, Grishin NV. Structural classification of zinc fingers. Nucleic Acids Res 2003;31:532–550.
39. Krissinel E, Henrick K. Secondary-structure matching (SSM), a new tool for fast protein structure alignment in three dimensions. Acta Crystallogr D Biol Crystallogr 2004;60:2256–2268.
40. Plambeck CA, Kwan AHY, Adams DJ, Westman BJ, van der Weyden L, Medcalf RL, Morris BJ, Mackay JP. The structure of the zinc finger domain from human splicing factor ZNF265 fold. J Biol Chem 2003;278:22805–22811.
41. Wang B, Alam SL, Meyer HH, Payne M, Stemmler TL, Davis DR, Sundquist WI. Structure and ubiquitin interactions of the conserved zinc finger domain of Npl4. J Biol Chem 2003;278:20225–20234.
42. Yu GW, Allen MD, Andreeva A, Fersht AR, Bycroft M. Solution structure of the C4 zinc finger domain of HDM2. Protein Sci 2006;15:384–389.
43. Higa MM, Alam SL, Sundquist WI, Ullman KS. Molecular characterization of the Ran-binding zinc finger domain of Nup153. J Biol Chem 2007;282:17090–17100.
44. Alam SL, Sun J, Payne M, Welch BD, Blake BK, Davis DR, Meyer HH, Emr SD, Sundquist WI. Ubiquitin interactions of NZF zinc fingers. EMBO J 2004;23:1411–1421.
45. Loughlin FE, Mansfield RE, Vaz PM, McGrath AP, Setiyaputra S, Gamsjaeger R, Chen ES, Morris BJ, Guss JM, Mackay JP. The zinc fingers of the SR-like protein ZRANB2 are single-stranded RNA-binding domains that recognize 5′ splice site-like sequences. Proc Natl Acad Sci USA 2009;106:5581–5586.